Published in final edited form as:
*Dev Cell*. 2010 July 20; 19(1): 66–77. doi:10.1016/j.devcel.2010.06.005.

# Pitchfork Regulates Primary Cilia Dizsassembly and Left-Right Asymmetry

**Doris Kinzel**[1,8], **Karsten Boldt**[2,7,8], **Erica E. Davis**[4], **Ingo Burtscher**[1], **Dietrich Trümbach**[3], **Bill Diplas**[4], **Tania Attié-Bitach**[5], **Wolfgang Wurst**[3], **Nicholas Katsanis**[4,6], **Marius Ueffing**[2,7], and **Heiko Lickert**[1,*]

[1]Institute of Stem Cell Research, Helmholtz Zentrum München, 85764 Neuherberg, Germany

[2]Department of Protein Science, Helmholtz Zentrum München, 85764 Neuherberg, Germany

[3]Institute of Developmental Genetics, Helmholtz Zentrum München, 85764 Neuherberg, Germany

[4]McKusick-Nathans Institute of Genetic Medicine, Johns Hopkins University School of Medicine, Baltimore, MD 21205, USA

[5]Département de Génétique et INSERM U-781, Hôpital Necker-Enfant Malades, 75015 Paris Cedex 15, France

[6]Center for Human Disease Modeling, Department of Cell Biology, Duke University, Durham, NC 27708, USA

[7]Division of Experimental Ophthalmology, Center of Ophthalmology, University of Tübingen, 72076 Tübingen, Germany

## SUMMARY

A variety of developmental disorders have been associated with ciliary defects, yet the controls that govern cilia disassembly are largely unknown. Here we report a mouse embryonic node gene, which we named *Pitchfork* (*Pifo*). Pifo associates with ciliary targeting complexes and accumulates at the basal body during cilia disassembly. Haploinsufficiency causes a unique node cilia duplication phenotype, left-right asymmetry defects, and heart failure. This phenotype is likely relevant in humans, because we identified a heterozygous R80K *PIFO* mutation in a fetus with situs inversus and cystic liver and kidneys, and in patient with double-outflow right ventricle. We show that PIFO, but not R80K PIFO, is sufficient to activate Aurora A, a protooncogenic kinase that induces cilia retraction, and that *Pifo*/*PIFO* mutation causes cilia retraction, basal body liberation, and overreplication defects. Thus, the observation of a disassembly phenotype in vivo provides an entry point to understand and categorize ciliary disease.

## INTRODUCTION

In addition to the well-known function of cilia in fluid transport and cell motility, it has been shown recently that sensory primary cilia are important for Hedgehog (Hh), Wnt, and PDGFα signal reception and transduction (Huangfu et al., 2003; Rohatgi et al., 2007; Schneider et al., 2005; Gerdes et al., 2007). As such, defects in cilia lead to a wide range of



*Correspondence: heiko.lickert@helmholtz-muenchen.de.
[8]These authors contributed equally to this work

**SUPPLEMENTAL INFORMATION**

Supplemental Information includes five figures, one table, six movies, Supplemental References, and Supplemental Experimental Procedures and can be found with this article online at doi:10.1016/j.devcel.2010.06.005.

human ciliary dysfunction syndromes, termed collectively the ciliopathies, including left-right (LR) asymmetry defects, male infertility, as well as polycystic kidney, liver, and pancreas disease (Michaud and Yoder, 2006; Badano et al., 2006). However, a more comprehensive understanding of the underlying mechanisms of ciliary disease requires the establishment of mouse models that allow studying different aspects of ciliogenesis, such as cilia assembly and disassembly.

Centrosomes are the major microtubule-organizing center (MTOC) in animal cells (Bettencourt-Dias and Glover, 2007). They are composed of two centrioles surrounded by microtubule (MT)-nucleating material, termed pericentriolar material (PCM). Centrioles duplicate during S phase in a semiconservative fashion with the mother centriole (MC), serving as a template for the formation of the daughter centriole (DC). Centrioles can either give rise to centrosomes, and in turn form the spindle pole during mitosis, or the MC can undergo a reversible conversion into a basal body and initiate the assembly of a primary cilium when cells enter growth arrest.

Cilia disassembly occurs when G0 growth-arrested cells reenter the cell cycle (Rieder et al., 1979; Tucker et al., 1979). During cilia disassembly, the centrioles duplicate in S phase and the basal body detaches from the plasma membrane (PM) to participate as centrosomes in mitotic-spindle assembly (Santos and Reiter, 2008). The current understanding of the cellular processes governing the early steps of cilia disassembly remains rudimentary, except that cilia retraction is regulated by the HEF1-AuroraA (AurA)-HDAC6 cascade (Pugacheva et al., 2007). In response to extracellular cues, the protooncogenic kinase AurA becomes activated at the basal body of the cilium in a HEF1-dependent fashion. This causes phosphorylation and activation of the tubulin deacetylase HDAC6, which culminates in destabilization of acetylated ciliary MTs (axoneme).

During cilia assembly and disassembly structural, functional, and regulatory proteins, which are synthesized elsewhere in the cell, have to be transported to the cilia (Pazour and Bloodgood, 2008). The process of delivering proteins from the Golgi to the cilium is likely to involve intraflagellar transport (IFT) proteins (Rosenbaum and Witman, 2002), Bardet-Biedl syndrome (BBS) proteins (Badano et al., 2006), and small GTPases of the Rab, Arf, and Arl subfamilies of the Ras superfamily (Gillingham and Munro, 2007). It is proposed that cascades of small GTPases regulate the budding of the carriers from the Golgi complex (Deretic, 2006), as well as transport and fusion of the carriers with the PM at the base of the cilium (Moritz et al., 2001). Ciliary targeting complexes are assembled in the *trans*-Golgi network (TGN) and ciliary localization depends on targeting sequences in ciliary proteins (Pazour and Bloodgood, 2008). The docking of cargo occurs at the transition zone between basal body and cilium, where the ciliary membrane forms a characteristic necklace region (Pedersen et al., 2008). While cilia assembly necessitates efficient vesicular transport from the Golgi to the cilium (Rosenbaum and Witman, 2002), it is less clear if this is also true for cilia disassembly.

In a microarray-based expression screen of *Foxa2* mutant embryos designed to identify mouse gastrula organizer genes implicated in embryonic pattern formation, we uncovered several node genes (Tamplin et al., 2008). Here, we describe the in-depth functional analysis of one of these genes, which we named *Pitchfork* (*Pifo*), and show its critical role in regulating cilia disassembly and a potential contribution of a variant to human ciliary disease.

# RESULTS

## Identification of *Pifo* as a Node and Ciliary Gene

We recently discovered a functionally nonannotated gene (*1700027A23Rik*), expressed specifically in the monociliated pit cells of the mouse node at embryonic day (E) 7.75 (Figures 1B–1D). Because of the important function of the node in LR pattern formation, we decided to generate a knockout allele to address the function of this gene in vivo. Based on the morphological features of mutant cilia (to be discussed in subsequent sections), we named the gene *Pifo* (accession numbers: HM237137–HM237140). *Pifo* contains three predicted independent promoters, which initiate transcription of two different mRNA isoforms (Figure S1A, available online) that encode proteins of 207 and 246 amino acids, respectively (Figure 1A). *Pifo* is highly conserved among chordates that have adopted the cilium for embryonic signaling (Huangfu and Anderson, 2006). The long Pifo isoform contains a predicted N-terminal coiled-coil domain (Figure 1A, dotted line) that is a common feature of centrosomal proteins (Andersen et al., 2003), but is not present in the human *PIFO* ortholog, *C1ORF88*. Both protein isoforms contain a domain of unknown function (DUF1309; Figure 1A, line; Figure S2).

To analyze Pifo in more detail, we raised two polyclonal rabbit antibodies against a conserved C-terminal epitope (Figure 1A, box). The specificity of the affinity-purified antibodies was verified by overexpressing GFP- or SF-TAP (Strep/FLAG-tandem affinity purification)-tagged (Gloeckner et al., 2007) long isoform Pifo protein in human embryonic kidney cells (HEK293T) or mouse NIH 3T3 cells followed by western blot analysis and immunocytochemistry (Figures S1J–S1M). The open reading frames of the long and short *Pifo* mRNA isoforms encode predicted proteins of 28.16 and 23.43 kDa, respectively. Using nuclear and cytoplasmic fractionation of adult testis lysates, we detected the long and short protein isoforms in the nuclear and cytoplasmic fraction, respectively, indicating that the N-terminal coiled-coil domain is important for nuclear localization (Figure S1L). Both protein isoforms migrated in line with their expected sizes, confirming that two different promoters drive the expression of a long and a short *Pifo* mRNA transcript in adult testis and that these isoforms are translated into differentially localized protein isoforms. Using immunoelectron microscopy (EM) we investigated the subcellular localization of Pifo in node cells at E7.5. The ultrastructural analysis revealed that the protein is localized in the nucleus, Golgi apparatus, and in vesicles of the TGN (Figure 1E). In addition, Pifo is found close to the ciliary membrane along the axoneme of the node pit cells (Figure 1F). Confocal immunofluorescent microscopy analysis also established that Pifo localizes to vesicles in the TGN and particles along the stabilized MTs of the sperm tail of adult spermatocytes (Figures 1G and 1H) and mouse node pit cells (Figures 1I and 1J). This pattern is reminiscent of the localization of some IFT and associated MT-motor proteins (Rosenbaum and Witman, 2002), as well as ciliary targeting complexes in the TGN (Pazour and Bloodgood, 2008). Taken together with the observation that *Pifo* mRNA is highly enriched in other ciliated tissues (McClintock et al., 2008), these results suggest a role for Pifo during ciliogenesis.

## Pifo Regulates Cardiac LR Asymmetry and Outflow Tract Remodeling

To evaluate Pifo in embryonic pattern formation, we generated a knockin of the *NLS-lacZ* (*nuclear localization sequence β-galactosidase*) gene in exon 1b of *Pifo*, removing all downstream coding exons (Figure S1B), which we confirmed by Southern blot analysis (Figures S1C and S1D). Three targeted embryonic stem (ES) cell clones were used to generate germ-line chimeras (n = 13). The *lacZ* reporter allele expression reflected the endogenous Pifo protein localization in spermatogonia of adult testis from diploid chimeric mice (Figures S1H and S1I) and embryonic lung mesenchyme from completely ES cell-

derived embryos (Figures S1F and S1G). β-galactosidase activity of the *Pifo*$^{lacZ/+}$ reporter allele and Pifo protein localization confirmed the expression of mRNA in tissues rich in ciliated cells, such as lung, kidney, and testis (Figures S1E–S1I and McClintock et al., 2008).

The low contribution of targeted ES cells to chimeras suggests a requirement for normal Pifo levels in the soma. Due to haploinsufficient male infertility of the chimera we were unable to generate a mouse line (D.K. and H.L., unpublished data); we therefore analyzed Pifo function during embryonic development using the tetraploid complementation approach (Nagy et al., 1993). *Pifo*$^{lacZ/+}$ mutants derived entirely from ES cells die due to congenital heart defects at E12.5 (Figure 2; n = 25). Cross-morphological and histological analysis revealed that all hearts showed double-outflow right ventricle (DORV) and right-ventricular hypoplasia (Figures 2A–2D). To understand the basis of this phenotype, we analyzed makers of outflow tract (OFT) development using in situ hybridization at E10.5. Mutations in *Pitx2* affect the alignment of the arterio-ventricular connections and cause DORV and ventricular hypolasia (Liu et al., 2002; Ai et al., 2006). The left-sided expressed *Pitx2c* isoform was specifically downregulated in the left OFT region, but expressed at normal levels in the left lateral wall of the right ventricle (Figures 2E and 2F). The failure to express *Pitx2c* is consistent with the phenotypic similarity between *Pitx2c*$^{-/-}$ and *Pifo*$^{lacZ/+}$ mutants (Liu et al., 2002). We also observed a reduction of *Bmp2* expression in the left OFT region (Figures 2G and 2H), but expression levels of *Bmp4* remained unchanged in the same region (data not shown). Neither cardiac dextral looping nor embryonic turning was affected, and unilateral gene expression of *Nodal*, *Lefty1/2*, and *Pitx2c* in the left lateral plate mesoderm in *Pifo*$^{lacZ/+}$ mutants was comparable to wild-type (WT) embryos at E8.5 (data not shown).

## Pifo Regulates Cilia Formation and LR Asymmetry at the Node

Recent studies have demonstrated that structural defects in node cilia formation or function lead to the failure of LR axis specification and affects cardiac looping, embryonic turning, and cardiac OFT remodeling (Hamada et al., 2002; Harvey, 2002). To analyze a possible function of Pifo in cilia formation, we focused on the mouse node and investigated cilia morphology by scanning EM (SEM) at E7.5 to E7.75 (Figures 3A–3G). WT embryos (n = 3) showed monociliated node cells in 99% of those analyzed (Figures 3A and 3G; n = 270). In contrast, *Pifo*$^{lacZ/+}$ embryos (n = 7) displayed multiple cilia defects in approximately half of the cilia analyzed (Figure 3G; n = 544). We categorized these cilia defects into five classes: duplication (Figure 3B), bifurcation (Figure 3C), partial bifurcation (Figure 3D), duplication and deformation (Figure 3E), and bulging (Figure 3F). We then compared the detailed ultrastructure of node cells in WT and *Pifo*$^{lacZ/+}$ mutants using transmission EM (TEM) at E7.5 to E7.75. WT primary node cilia are motile and show a 9 + 0 MT doublet architecture around the cilia periphery (Figure 3J; Fliegauf et al., 2007). In contrast, some of the mutant cilia show a nonparallel alignment of the MT doublets along the longitudinal axis of the ciliary axoneme (Figures 3H and 3I) and disturbed 9 + 0 architecture (Figures 3K and 3L). The architectural defects possibly result from a failure of the basal body to function as the MTOC and nucleate, or organize, the axonemal MTs.

The activation of the left-specific Nodal/TGFβ-signaling cascade depends on the “nodal flow” and thus on functional node cilia (Hamada et al., 2002). To test if the structural defects of *Pifo*$^{lacZ/+}$ cilia affect LR pattern formation at the node, we performed in situ hybridization for the earliest LR-specific marker genes. The Nodal/TGFβ-antagonist, *Cerr2* (Marques et al., 2004), and the ligand, *Nodal* (Lowe et al., 1996; Collignon et al., 1996), showed a bilateral asymmetric horseshoe-like expression pattern in crown cells surrounding the monociliated pit cells of the node in WT embryos (Figures 3M–3O). In contrast, *Pifo*$^{lacZ/+}$ mutants presented a disturbed horseshoe-like pattern and failed to asymmetrically express *Nodal* and *Cerr2* at the early somite stage (Figures 3P–3R). Consistent with these

findings, SEM analysis revealed that the overall node architecture was slightly disrupted (Figures S3A and S3B). These results indicate that structural node and cilia defects disturb LR patterning, initiating at the node. This is most likely the cause of the LR-patterning defects observed in the OFT (Figure 2) because *Pifo* mRNA is not expressed in other tissues at detectable levels until E9.5 (Figures S3C–S3H).

## Identification of Human PIFO Mutations in Laterality Syndromes and Ciliopathies

The LR asymmetry defects observed in $Pifo^{lacZ/+}$ embryos, due to abnormal ciliary structure, made *PIFO* a candidate contributor to ciliary disease in humans with hallmark LR defects such as situs inversus. We therefore screened all six coding exons and their respective splice junctions in the human *Pifo* ortholog, *C1ORF88*, in a cohort of 174 individuals diagnosed with Meckel-Gruber syndrome (MKS) or MKS-like phenotypes (combined n = 114) or Jeune Asphyxiating Thoracic Dystrophy (JATD; n = 60); both clinical categories represent phenotypically severe ciliopathies with documented LR abnormalities (Badano et al., 2005). We also sequenced patients or fetuses with laterality defects, DORV, or both (n = 32). Interestingly, we found the same heterozygous R80K-encoding variant in two cases: one sporadic neonatal lethal case with thoracic-abdominal situs inversus, cystic kidneys, and liver fibrosis, and a patient with isolated DORV. Importantly, this allele was absent from 312 ethnically matched control chromosomes of Northern European descent and changes a rigidly conserved arginine residue which is evolutionarily conserved from *C. intestinalis* to mammals (Figure 1A). Taken together, these results suggest that *PIFO* is a rare contributor to total mutational load in ciliopathies for which pathogenic alleles may only be present in heterozygosity.

## Pifo Accumulates Specifically at the Basal Body and Ciliary Necklace during the Early Phase of Cilia Assembly and Disassembly

To understand how *Pifo* haploinsufficiency can lead to ciliary defects, we examined Pifo localization at the mouse node. The node is an ideal in vivo model for the study of cilia assembly and disassembly (Figure 4A, boxed area) as it contains a ventral epithelial layer of monociliated pit cells (Figure 4A, red cells) and a dorsal epithelial layer of nonciliated, proliferating epiblast cells that divide toward the amniotic cavity (Figure 4A, purple cell). Live-cell imaging revealed that pit cells are derived from dorsal node epiblast cells that leave the epithelial layer and enter G0 (I.B. and H.L., unpublished data). These primary cilia-assembling cells are found in an intermediate zone between the ventral and dorsal epithelial layer (Figure 4A, green cell). Furthermore, monociliated pit cells can re-enter the cell cycle in the ventral node epithelium (Figure 4A, yellow cell). Using immunohistochemistry and confocal imaging, we analyzed colocalization of Pifo with the centriole marker Cep135 (Kleylein-Sohn et al., 2007) and the basal body marker Cep164 (Graser et al., 2007). We found Pifo colocalizes with the primary cilia assembly protein Cep164 in cilia-forming intermediate cells (Figure 4B, green arrowheads), but was conspicuously absent from the basal body that nucleates the axonemal MTs of the primary ciliated pit cells (Figure 4B, II, red arrowheads); we obtained similar results for the centriole MT organizing protein Cep135 (Figure 4C). High-resolution confocal microscopy confirmed the colocalization of Pifo with the centriolar and basal body proteins in cilia-assembling intermediate cells and cilia-disassembling mitotic pit cells (Figure 4D). Furthermore, confocal sections parallel to the plane of the apical plasma membrane of ventral pit cells revealed that Pifo appears in a ciliary necklace-like pattern (Pedersen et al., 2008), which resembles the cargo-docking site for ciliary transport (Figure 4E). Pifo localizes apically to the adherens junction marker E-Cadherin and at the ciliary necklace, where it colocalizes with the microtubule transport protein Kif3a, the centriolar protein, Cep135, and in some cells with the activated form of AurA (Figure 4E). These data demonstrate that Pifo accumulates specifically at the basal body and ciliary necklace during

the early steps of cilia assembly and disassembly, when structural, functional, and regulatory proteins are delivered to cilia.

## Pifo Associates with Ciliary Targeting Complexes

Haploinsufficiency for *Pifo* leads to a unique cilia duplication phenotype at the mouse node not seen in other cilia mutants, which usually show absent, small, or bulged cilia (Eggenschwiler and Anderson, 2007). To understand how this duplication phenotype arises, we studied Pifo localization and function in cell culture, where we could analyze different phases of cilia assembly and disassembly (Pugacheva et al., 2007; Ocbina and Anderson, 2008). Guided by the expression of Pifo in the limb bud (Figure S4), we prepared primary limb cultures (PLC) from E11.5 embryos. In low-density cultures and in the presence of serum, mesenchymal PLC cells proliferate for several passages until they enter senescence. Under these conditions, PLC cells rarely form primary cilia and do not synthesize Pifo during either interphase or mitosis (Figure 5A, I, and data not shown). However, high-density culture and serum deprivation leads to rapid cell cycle exit and induction of cilia assembly. Pifo vesicles accumulate in the cytoplasm (Figure 5A, II) and localize to both the TGN and the growing axoneme (Figure 5A, III). In G0-deprived primary ciliated cells, Pifo localizes to the TGN and to the basal body (Figure 5A, IV) before levels gradually decrease such that it is rarely observed at the centriole (Figure 5A, V). Restimulation of G0 cells leads to rapid cilia disassembly and highly synchronous progression through each stage of the cell cycle. Pifo accumulates in vesicles at cell cycle reentry in S phase (Figure 5A, VI) and declines during mitosis (Figure 5A, VII). We noticed that Pifo accumulation was greatest in the early phase of ciliary disassembly (Figure 7G and data not shown), which let us to investigate the nature of these vesicles. We found that Pifo vesicles budding from the *cis*-Golgi network (Figure 5C), colocalized with the MT network and in parcels along the cilium (Figure 5B) and partially colocalized with EEA1-positive early endosomes (Figure 5D) and the TGN and endosome marker M6PR (Figure 5E). To confirm these results and to seek further evidence that Pifo is involved in vesicular trafficking to the cilium and basal body, we used high-resolution single-cell imaging in stable transfected mouse IMCD3 kidney cells. During early cilia disassembly (Figure 5F, G0 + 2 hr serum), Venus-tagged PIFO is transported in parcels along the Arl13b-positive cilium (Movies S1–S3). Later during cilia disassembly after the cilium is resorbed (Figure 5F, G0 + 4 hr serum), PIFO-Venus transport vesicles are accumulating in the cytoplasm (Movies S4–S6). To analyze if Pifo is involved in MT-dependent vesicular trafficking we tested physical interactions in HEK293T cells, which assemble and disassemble cilia upon serum starvation and restimulation, respectively (Figures S5A–S5D). We precipitated endogenous proteins using immobilized mouse and human SF-TAP-tagged PIFO in ciliated and cilia-disassembling HEK293T cells. This pull-down analysis revealed that the early endosome marker Rab6, the late endosome marker Rab8, the cilium localized small GTPase Arl13b (Caspary et al., 2007), the PCM protein γ-Tubulin, the centriolar protein Centrin, the MT protein β-Tubulin, and the motor protein Kif3a, all physically interact with Pifo/PIFO in cell culture (Figure 5G and Figures S5E–S5H). Furthermore, these interactions are dependent to various degrees on the presence of the N-terminal coiled-coil region of Pifo (Figures S5E–S5H). Taken together, these data show that mouse and/or human PIFO colocalizes and physically interact with vesicular targeting complexes, suggesting a function in ciliary transport.

## Pifo Controls Centrosome Liberation and Duplication during Cilia Disassembly

We next asked at which step of ciliogenesis Pifo functions and prepared PLC from E11.5 WT and $Pifo^{lacZ/+}$ embryos. In high-density cultures, serum deprivation for 48 hr induced primary cilia formation in >80% of WT and $Pifo^{lacZ/+}$ cells (data not shown), demonstrating that haploinsufficiency for *Pifo* does not block cilia assembly per se (Figures 6A and 6F). In contrast, G0 primary ciliated $Pifo^{lacZ/+}$ PLC cells that reentered mitosis after mitogenic

stimulation (Figure 6K) showed a high percentage of mitotic defects (Figure 6L) during cilia disassembly. Consistent with our phenotype at the mouse node, we found cells with duplicated cilia after cytokinesis (Figures 6D and 6I). The cause of the duplicated cilia phenotype was the overproduction of centrosomes during S phase, with defects already observed in prophase cells (compare Figures 6B and 6G). Centrosome overreplication leads to the formation of multipolar spindles during metaphase and anaphase (Figures 6C and 6H). To exclude a general function for Pifo in mitosis we investigated pluripotent and proliferating ES cells that contain 10%–15% primary ciliated cells. ES cells divide rapidly in culture and we observed mitotic defects in only 2.5% of all mitoses (Figures 6E and 6J). These data together with the specific expression in ciliated cells suggest that Pifo is not generally important for centrosome duplication, cell cycle progression, and mitosis in proliferating cells. To understand the molecular details of the centrosome overreplication phenotype, we investigated the cilium and the basal body in primary ciliated cells reentering the cell cycle in cell culture and in vivo (Figures 6N–6P). In WT cells, retraction of the cilium occurs before mitosis in node (Figure 6N) and PLC cells (Figure 6Q), as has been reported for other cell types (Pugacheva et al., 2007). In $Pifo^{lacZ/+}$ node (Figures 6O and 6P) and PLC cells (Figures 6R and 6S) the basal body fails to disconnect from the cilium and the cilium is retained during mitosis in PLCs (Figure 6M). This underlines the function of Pifo during cilia disassembly and indicates that it is required specifically to control cilia retraction as well as the liberation and duplication of the basal body/centrosome during primary cilia disassembly.

## PIFO Is Sufficient to Enhance AurA Activation during Cilia Disassembly

During cilia disassembly, the stabilized, acetylated MTs of the ciliary axoneme are deacetylated and destabilized in an AurA-HDAC6-dependent process (Pugacheva et al., 2007). Colocalization of activated AurA kinase (phAurA) and Pifo at the basal body/ciliary necklace region of a few, presumably cilia-disassembling node cells (Figure 4E), in addition to the absence of both proteins at the majority of basal bodies near a well-formed cilium (Figures 4B and 4C and Pugacheva et al., 2007), suggested to us that Pifo could possibly regulate AurA activity during cilia disasssembly. To test this hypothesis, we first analyzed the localization of PIFO-Venus in cilia-disassembling stably transfected IMCD3 cells. Restimulation of G0 cells led to rapid accumulation of PIFO-Venus at the basal body/centrosome (Figures 7A and 7B), which is analogous to activated phAurA (Pugacheva et al., 2007). Second, we precipitated endogenous AurA using immobilized human SF-TAP-tagged PIFO and R80K PIFO in G0 and cilia-disassembling HEK293T cells. This pull-down analysis revealed that both WT and R80K PIFO physically interact with endogenous AurA (Figure 7C). To test if PIFO regulates AurA activity, we analyzed the phosphorylation status of AurA in transiently transfected HEK293T cells. As compared to hTERT-RPE1, IMCD3, and Caki-1 cells (Pugacheva et al., 2007), SF-TAP-tag mock-transfected HEK293T cells show peak levels of AurA activation 2 hr after serum stimulation (Figure 7D). Strikingly, overexpression of SF-TAP-PIFO during the early phase of cilia disassembly leads to a prolonged activation of AurA, whereas total AurA levels were largely unaffected (Figure 7E). In contrast, overexpression of TAP-R80K PIFO completely blocked AurA phosphorylation (Figure 7F), although the missense mutation had no impact on protein stability (Figures 7E and 7F, compare α-Flag blots) and physical interaction with AurA (Figure 7C). We noticed that the accumulation of SF-TAP-PIFO during the process of cilia disassembly was most likely due to posttranscriptional and perhaps cell cycle-dependent regulation (Figure 7G). Taken together, these results indicate that mouse and human PIFO accumulate in a cell cycle-dependent manner at the basal body to activate AurA, a process that is specifically abolished by the R80K mutation.

Inhibition of AurA activation by knockdown or small molecule inhibitors lead to failure in cilia disassembly and appearance of mitotically arrested cells possessing both spindles and cilia (Pugacheva et al., 2007). To test if the PIFO R80K-mediated AurA inhibition had a similar impact on cilia disassembly we transiently transfected SF-TAP-tagged WT and R80K PIFO into PLC cells which express endogenous Pifo (Figure 5A). Detailed analysis of cilia disassembly in TAP-tagged or SF-TAP PIFO overexpressing cells revealed that cilia retraction occurred concurrent with centriole duplication (Figure 7H, I–IV). After centrosome splitting cilia were detached from the basal body/centrosome (Figure 7H, IV). In contrast, overexpression of the SF-TAP-tagged R80K PIFO protein caused dominant centriole overreplication as well as the failure of cilia retraction and centriole liberation during cilia disassembly (Figures 7H, V–VIII, and 7I), which is analogous to the *Pifo* haploinsufficient mouse (Figures 6). These results indicate that PIFO regulates AurA and is required for several aspects of cilia disassembly.

## DISCUSSION

We have identified *Pifo* as a gene whose product regulates LR pattern formation, with potential involvement in human congenital heart disease and ciliary dysfunction syndromes. In contrast to other ciliary mutations that affect cilia formation per se, Pifo mutants represent, to our knowledge, the first example showing a cilia duplication phenotype at the mouse node. This highlights the fact that Pifo is a cilia disassembly protein that specifically controls basal body detachment as well as centrosome duplication and ciliary retraction in regions of embryonic organizer activities.

The process of cilia disassembly is poorly understood, but it is clear that release of the basal body to act in spindle-pole assembly is central to cell division (Badano et al., 2005; Bettencourt-Dias and Glover, 2007; Michaud and Yoder, 2006). Our data suggest that during cilia disassembly three major processes occur: first, the retraction of the cilium; second, the duplication of the centrioles; and third, the dislodging of the basal body from the cilium. Ciliary retraction has been shown to be dependent on the HEF1-AuroraA-HDAC6 cascade (Pugacheva et al., 2007). Inhibition of AurA causes appearance of mitotically arrested cells possessing both spindles and cilia, indicating that AurA has an additional function in basal body detachment and centriole duplication. Likewise, suboptimal levels of Pifo prevent cilia retraction as well as basal body detachment and causes appearance of cells possessing both spindles and cilia. We confirmed that Pifo, comparable to activated AurA, specifically accumulates at the basal body and that both proteins physically interact during cilia disassembly. Moreover, we were able to demonstrate that WT PIFO enhances, whereas R80K PIFO blocks AurA activation. Thus, these results indicate that ciliary retraction and centriole liberation are tightly associated cellular events during cilia disassembly, which are both regulated by PIFO and AurA at the basal body. Failure to dislodge the centriole from the cilium might cause secondary defects leading to centriole amplification, a process that is normally under the control of several kinases, such as Cyclin-dependent kinase-2, Polo-like kinase 4, and others (Bettencourt-Dias and Glover, 2007). An equally parsimonious idea is that PIFO directly or indirectly regulates cell cycle-dependent kinases, a hypothesis, which now has to be tested more directly. In our initial attempts to build a PIFO protein interaction network, we identified the cell cycle kinase inhibitor p16Ink4a as a potential protein-protein interaction partner (data not shown). Interestingly, loss of p16Ink4a generates supernumerary centrosomes through centriole pair splitting (McDermott et al., 2006), a phenotype very similar to that observed during the early phase of cilia disassembly.

How PIFO and AurA regulate basal body dislodgement from the cilium is less clear. Failure of ciliary retraction and destabilization of the axoneme might be a prerequisite for centriole liberation. Another possibility is that structural and functional proteins are actively delivered

to, or displaced from the basal body. Interestingly, the Pifo domain of unknown function (DUF1309) is only found in a few proteins, including Outer dense fiber3 (Odf3) and Odf3 like (Figure S2). The Odf family members were identified as major components of the sperm-tail cytoskeleton (Petersen et al., 1999). Odf2, also known as hCenexin1, was proposed to be a crucial distal/subdistal appendage protein of the mother centriole essential for nucleation of axonemal MT and anchoring of the basal body to the PM (Ishikawa et al., 2005). Interestingly, Pifo and Odf3 colocalize to regions distinct to Odf2 at the sperm tail (Egydio de Carvalho et al., 2002 and data not shown), which could indicate that competitive inhibition or displacement of proteins could be a mechanism that regulates basal body anchoring and detachment. Interestingly, stable shRNA knockdown of the MKS genes, *Mks1* and *Mks3*, in IMCD3 cells induced multiciliated and multicentrosomal phenotypes (Tammachote et al., 2009), and it was suggested that MKS proteins function in basal body migration and/or docking at the PM (Dawe et al., 2007). Our analysis demonstrates how such a multiciliated and multicentrosomal phenotype develops during cilia disassembly and suggests that MKS proteins could be involved in basal body detachment. In summary, our data supports the previous hypothesis that disassembly of the primary cilium and liberation of its captive basal body are essential for cell division. A failure of proper cilia disassembly can result in multipolar spindles, and in consequence aneuploidy, which in the context of multistage carcinogenesis contributes to malignancy.

We hypothesize that Pifo regulates cilia disassembly by directing structural, functional, or regulatory proteins to the basal body. It has been suggested that IFT proteins, BBS proteins, and small GTPases of the Rab, Arf, and Arl subfamilies are all involved in the delivery of proteins to the cilia. We show that Pifo colocalizes and/or physically interacts with Rab6, Rab8, Rab11, Arl13b, β-, γ-Tubulin, Centrin, and the MT-motor protein Kif3a, indicating that Pifo is involved in ciliary transport. We have confirmed this by live-cell imaging. Together with the observation that depletion of IFT proteins in *Chlamydomas* and mammals interferes with cilia disassembly (Pan and Snell, 2005; Pugacheva et al., 2007), the function of ciliary transport seems phylogenetically conserved, and possibly serves to deliver functional and regulatory proteins to the basal body.

Importantly, Pifo cannot be part of a general regulatory mechanism for cilia disassembly for two reasons: first, ciliary proteins are well conserved during evolution—the best understood of which are found in *Chlamydomonas*; and second, if a protein is generally important for ciliogenesis it would be expressed in all ciliated cells of the organism. Pifo appears with chordates and is expressed specifically in regions of embryonic organizing activities, such as the mouse node, the floorplate of the neural tube, the apical ectodermal ridge, and the growth zone of the embryonic limb bud (Figure S4). These organizer regions are important for embryonic patterning and are a source of differentiation and proliferation signals. Primary cilia are important sites for reception of Wnt, Hh, and PDGF signals (Eggenschwiler and Anderson, 2007), but it is currently not known how a cell decides to either proliferate or differentiate in response to these signals. Disassembly and retraction of cilia occurs upon entry into mitosis. Thus, proteins regulating cilia disassembly might allow cell proliferation instead of differentiation and influence the cell type-specific response to an environmental signal. Indeed, we believe that Pifo is specifically expressed in response to environmental signals and represents an evolutionary adaptation to primary cilia signaling and embryonic patterning. However, it is unlikely that Pifo is major bona fide ciliopathy gene, an observation consistent with the severe developmental phenotypes observed in the mouse mutant. It is tempting to speculate that the R80K mutation found in human represents a dominant allele, especially since expression of the mutant protein alone was sufficient to induce morphological ciliary phenotypes. Unfortunately, the lack of parental material precludes testing of this idea. An equally parsimonious hypothesis is that this mutation likely contributes to the ciliary phenotypes observed in the patients in concert with alleles at

other ciliopathy loci, as shown previously (Leitch et al., 2008; Khanna et al., 2009). Mutational screening of *PIFO* in much larger cohorts with or without known primary disease loci, however, will be necessary to substantiate this hypothesis. Overall, our study provides novel insight into the molecular process of cilia disassembly and provides an entry point to understand primary cilia signaling and cell cycle control in the mouse model.

## EXPERIMENTAL PROCEDURES

### ES Cell Culture and Generation of the Pifo$^{lacZ/+}$ Allele and Expression Constructs

All primers are listed in Table S1. The knockin construct was designed as shown in Figure S1B and the construction including expression vectors is described in the Supplemental Information. F1 ES cells (IDG3.2) were electroporated with AscI-linearized pL254 Pifo-NLS-lacZ-neo targeting vector. Neomycin-resistant clones were selected with 300 μg/ml G418 (Invitrogen). Homologous recombination at the *Pifo* locus was confirmed by Southern blot analysis using a 3′ probe amplified by PCR (3′-probe fwd; 3′-probe rev) and an internal lacZ probe (lacZ-probe-fwd; lacZ-probe-rev) as indicated in Figure S1B. Three homologous recombined ES cell clones were injected into C57Bl/6 blastocyts to obtain chimeras.

### Generation of Completely ES Cell-Derived Embryos

Tetraploid embryos were generated by electrofusion of two-cell-stage embryos (Nagy et al., 1993) using ubiquitous dsRed expressing embryos isolated from donor females (Vintersten et al., 2004). Two 3–4 cell stage tetraploid embryos were aggregated with clumps of six to eight *Pifo*$^{lacz/+}$ ES cells overnight and blastocysts were transferred into the uterus of recipients. After dissection, the contribution of tetraploid cells to the completely ES cell-derived embryos was examined using a Zeiss Stereo Lumar.V12 fluorescent microscope.

### Transmission and SEM

For SEM, embryos were fixed in 1% glutaraldehyde in phosphate-buffered saline (PBS) overnight, then treated using standard procedures and analyzed with a Jeol (JSM-6300F) microscope. For TEM, embryos were fixed in 2.5% glutaraldehyde in cacodylate buffer. Embryos were treated using standard procedures and analyzed by TEM (EM10CR, Zeiss).

### In Situ Hybridization Analysis

Whole-mount in situ hybridization was performed as previously described and the *Pifo* mRNA probe was transcribed from a sequence-verified cDNA clone (Tamplin et al., 2008). Embryos were imaged using a Zeiss Stereo Lumar.V12 microscope. After whole-mount in situ hybridization embryos were dehydrated with methanol and embedded in paraffin using standard procedures. Paraffin blocks were sectioned at 8 μm, mounted on glass slides, dewaxed, and stained for microscopy.

### Immunohistochemistry and Imaging

Immunofluorescence whole mounts of embryos isolated at E7.5 to E7.75 was performed as previously described (Burtscher and Lickert, 2009). For limb culture or ES cell immunostaining, cells were fixed for 5 min with 4% paraformaldehyde (PFA) in PBS and then permeabilized in ice-cold methanol for 5 min. After blocking in PBS with 10% sheep serum, 1% bovine serum albumin for 30 min, cells were incubated in blocking solution with the primary antibody overnight at 4°C. Antibodies were used at the following concentrations: 1:250 acetylated-Tubulin (Sigma), 1:250 Kif3a (BD Bioscience), 1:250 γ-Tubulin (Sigma), 1:100 Cy3-coupled Cep135 and Cep164 (gifts from Erich Nigg's lab), 1:50 affinity-purified Pifo (Pineda, Berlin, Germany), 1:250 GM130 (BD), 1:100 EEA1

(BD), 1:100 M6PR (Abnova), 1:250 AurA, and phAurA (NEB). After incubation with secondary antibodies embryos were embedded between coverslips using 120 μm Secure-Seal™ spacers (Invitrogen, S24737) and ProLong Gold antifade reagent with 4′,6-diamidin-2′-phenylindol-dihydrochlorid (DAPI; Invitrogen). An Olympus FV1000 laser-scanning confocal microscope (63× objective) with optical sections of 0.49 μm was used for static analysis and a Zeiss Observer microscope was used for live-cell imaging.

### Primary Limb Bud Cell Culture

The forelimbs of E12.5 *WT* or $Pifo^{lacz/+}$ embryos were dissected and disaggregated in 1× 0.05% Trypsin-EDTA. During 15 min incubation at 37°C the tissue was dissociated by pipette. The cell suspension was resuspended in Dulbecco's modified Eagle's medium (Invitrogen), supplemented with 15% fetal calf serum, 2 mM L-Glutamine (Invitrogen), and 1% penicillin/streptomycin, and seeded into a 96-well plate. To expand the primary limb bud culture the cells were split every two days.

### Immunoprecipitation and Immunoblotting

**StrepII Tag Affinity Purification—**The StrepII tag affinity purification was performed as previously described (Gloeckner et al., 2007).

### Western Blotting

Western blot analysis was performed by standard procedures. Antibodies were used in the following concentrations; 1:250 affinity-purified Pifo (Pineda), 1:1000 FLAG (Sigma), 1:1000 γ-Tubulin (Sigma), 1:1000 Rab6 (Santa Cruz), 1:1000 Rab8 (BD/RD), 1:1000 Arl13b (gift from Kenji Kontani), 1:1000 Kif3a (BD), 1:1000, β-tubulin (Sigma), 1:2000 Centrin (Abcam), 1:1000 AurA, and phAurA (NEB). Protein bands were visualized with ECL chemiluminescence (GE Healthcare) using hyperfilm (GE Healthcare).

### Ciliopathy Cases and Mutational Analysis

DNA from affected individuals and Northern European controls was extracted from tissue biopsies, blood, or lymphoblast cell lines according to standard procedures following informed consent. We PCR amplified the coding regions and intron-exon junctions of *PIFO* and subsequently carried out bidirectional sequencing using Big Dye Terminator v3.1 chemistry and an ABI3100 sequencer (Applied Biosystems) according to manufacturer's instructions. Sequences were aligned with Sequencher (Gene Codes), and chromatograms were assessed visually. Primer sequences are available upon request.

## Supplementary Material

Refer to Web version on PubMed Central for supplementary material.

## Acknowledgments

We are extremely grateful to W. Barkey and A. Theis for excellent technical assistance and P. Giallonardo for generation of chimeras. We thank D. Bonnet for DNA samples from DORV patients; L. Jennen for expert help with TEM; E. Nigg for Cep135 and Cep164; K. Kontani and T. Caspary for Arl13b antibodies; C.C. Hui for advice with primary limb bud cultures; B. Bruneau for *Bmp2*, *Bmp4*, and *Pitx2c* and H. Hamada for *Cerr2*, *Nodal*, and *Lefty1/2* in situ hybridization probes; and P. Liao, E. Drew, M. Goetz, M.J. Plevin, and N. Chadderton for their valuable comments on the manuscript. This work was supported by BMBF Quant Pro (FZK0316865A to M.U.), BMBF Systec-Dynamo (FZK 031155514 to M.U.), and EU 7th FW grant Affinomics (grant agreement no. 241481 to M.U.). This work was also supported by the Helmholtz Society, European Research Council, and German Research Foundation (DFG) with an Emmy-Noether fellowship and a starting grant awarded to H.L.; National Institute of Child Health and Development Grant R01HD04260 (N.K.); National Institute of Diabetes, Digestive, and Kidney Disorders Grants R01DK072301 and R01DK075972 (N.K.); National Research Service Award Fellowship F32 DK079541 (E.E.D.); the Macular Vision Research Foundation (N.K.); EU grant ProteomeBinders (FP6-026008)

(M.U.); the German Federal Ministry of Education and Research (BMBF: DYNAMO, FKZ: 0315513A) (M.U.); and the Kerstan Foundation (M.U.).

## References

Ai D, Liu W, Ma L, Dong F, Lu MF, Wang D, Verzi MP, Cai C, Gage PJ, Evans S, et al. Pitx2 regulates cardiac left-right asymmetry by patterning second cardiac lineage-derived myocardium. Dev Biol. 2006; 296:437–449. [PubMed: 16836994]

Andersen JS, Wilkinson CJ, Mayor T, Mortensen P, Nigg EA, Mann M. Proteomic characterization of the human centrosome by protein correlation profiling. Nature. 2003; 426:570–574. [PubMed: 14654843]

Badano JL, Teslovich TM, Katsanis N. The centrosome in human genetic disease. Nat Rev Genet. 2005; 6:194–205. [PubMed: 15738963]

Badano JL, Leitch CC, Ansley SJ, May-Simera H, Lawson S, Lewis RA, Beales PL, Dietz HC, Fisher S, Katsanis N. Dissection of epistasis in oligogenic Bardet-Biedl syndrome. Nature. 2006; 439:326–330. [PubMed: 16327777]

Bettencourt-Dias M, Glover DM. Centrosome biogenesis and function: centrosomics brings new understanding. Nat Rev Mol Cell Biol. 2007; 8:451–463. [PubMed: 17505520]

Burtscher I, Lickert H. Foxa2 regulates polarity and epithelialization in the endoderm germ layer of the mouse embryo. Development. 2009; 136:1029–1038. [PubMed: 19234065]

Caspary T, Larkins CE, Anderson KV. The graded response to Sonic Hedgehog depends on cilia architecture. Dev Cell. 2007; 12:767–778. [PubMed: 17488627]

Collignon J, Varlet I, Robertson EJ. Relationship between asymmetric nodal expression and the direction of embryonic turning. Nature. 1996; 381:155–158. [PubMed: 8610012]

Dawe HR, Smith UM, Cullinane AR, Gerrelli D, Cox P, Badano JL, Blair-Reid S, Sriram N, Katsanis N, Attie-Bitach T, et al. The Meckel-Gruber Syndrome proteins MKS1 and meckelin interact and are required for primary cilium formation. Hum Mol Genet. 2007; 16:173–186. [PubMed: 17185389]

Deretic D. A role for rhodopsin in a signal transduction cascade that regulates membrane trafficking and photoreceptor polarity. Vision Res. 2006; 46:4427–4433. [PubMed: 17010408]

Eggenschwiler JT, Anderson KV. Cilia and developmental signaling. Annu Rev Cell Dev Biol. 2007; 23:345–373. [PubMed: 17506691]

Egydio de Carvalho C, Tanaka H, Iguchi N, Ventela S, Nojima H, Nishimune Y. Molecular cloning and characterization of a complementary DNA encoding sperm tail protein SHIPPO 1. Biol Reprod. 2002; 66:785–795. [PubMed: 11870087]

Fliegauf M, Benzing T, Omran H. When cilia go bad: cilia defects and ciliopathies. Nat Rev Mol Cell Biol. 2007; 8:880–893. [PubMed: 17955020]

Gerdes JM, Liu Y, Zaghloul NA, Leitch CC, Lawson SS, Kato M, Beachy PA, Beales PL, DeMartino GN, Fisher S, et al. Disruption of the basal body compromises proteasomal function and perturbs intracellular Wnt response. Nat Genet. 2007; 39:1350–1360. [PubMed: 17906624]

Gillingham AK, Munro S. The small G proteins of the Arf family and their regulators. Annu Rev Cell Dev Biol. 2007; 23:579–611. [PubMed: 17506703]

Gloeckner CJ, Boldt K, Schumacher A, Roepman R, Ueffing M. A novel tandem affinity purification strategy for the efficient isolation and characterisation of native protein complexes. Proteomics. 2007; 7:4228–4234. [PubMed: 17979178]

Graser S, Stierhof YD, Lavoie SB, Gassner OS, Lamla S, Le Clech M, Nigg EA. Cep164, a novel centriole appendage protein required for primary cilium formation. J Cell Biol. 2007; 179:321–330. [PubMed: 17954613]

Hamada H, Meno C, Watanabe D, Saijoh Y. Establishment of vertebrate left-right asymmetry. Nat Rev Genet. 2002; 3:103–113. [PubMed: 11836504]

Harvey RP. Patterning the vertebrate heart. Nat Rev Genet. 2002; 3:544–556. [PubMed: 12094232]

Huangfu D, Anderson KV. Signaling from Smo to Ci/Gli: conservation and divergence of Hedgehog pathways from Drosophila to vertebrates. Development. 2006; 133:3–14. [PubMed: 16339192]

Huangfu D, Liu A, Rakeman AS, Murcia NS, Niswander L, Anderson KV. Hedgehog signalling in the mouse requires intraflagellar transport proteins. Nature. 2003; 426:83–87. [PubMed: 14603322]

Ishikawa H, Kubo A, Tsukita S, Tsukita S. Odf2-deficient mother centrioles lack distal/subdistal appendages and the ability to generate primary cilia. Nat Cell Biol. 2005; 7:517–524. [PubMed: 15852003]

Khanna H, Davis EE, Murga-Zamalloa CA, Estrada-Cuzcano A, Lopez I, den Hollander AI, Zonneveld MN, Othman MI, Waseem N, Chakarova CF, et al. A common allele in RPGRIP1L is a modifier of retinal degeneration in ciliopathies. Nat Genet. 2009; 41:739–745. [PubMed: 19430481]

Kleylein-Sohn J, Westendorf J, Le Clech M, Habedanck R, Stierhof YD, Nigg EA. Plk4-induced centriole biogenesis in human cells. Dev Cell. 2007; 13:190–202. [PubMed: 17681131]

Leitch CC, Zaghloul NA, Davis EE, Stoetzel C, Diaz-Font A, Rix S, Alfadhel M, Lewis RA, Eyaid W, Banin E, et al. Hypomorphic mutations in syndromic encephalocele genes are associated with Bardet-Biedl syndrome. Nat Genet. 2008; 40:443–448. [PubMed: 18327255]

Liu C, Liu W, Palie J, Lu MF, Brown NA, Martin JF. Pitx2c patterns anterior myocardium and aortic arch vessels and is required for local cell movement into atrioventricular cushions. Development. 2002; 129:5081–5091. [PubMed: 12397115]

Lowe LA, Supp DM, Sampath K, Yokoyama T, Wright CV, Potter SS, Overbeek P, Kuehn MR. Conserved left-right asymmetry of nodal expression and alterations in murine situs inversus. Nature. 1996; 381:158–161. [PubMed: 8610013]

Marques S, Borges AC, Silva AC, Freitas S, Cordenonsi M, Belo JA. The activity of the Nodal antagonist Cerl-2 in the mouse node is required for correct L/R body axis. Genes Dev. 2004; 18:2342–2347. [PubMed: 15466485]

McClintock TS, Glasser CE, Bose SC, Bergman DA. Tissue expression patterns identify mouse cilia genes. Physiol Genomics. 2008; 32:198–206. [PubMed: 17971504]

McDermott KM, Zhang J, Holst CR, Kozakiewicz BK, Singla V, Tlsty TD. p16(INK4a) prevents centrosome dysfunction and genomic instability in primary cells. PLoS Biol. 2006; 4:e51. [PubMed: 16464125]

Michaud EJ, Yoder BK. The primary cilium in cell signaling and cancer. Cancer Res. 2006; 66:6463–6467. [PubMed: 16818613]

Moritz OL, Tam BM, Hurd LL, PerÌnen J, Deretic D, Papermaster DS. Mutant rab8 impairs docking and fusion of rhodopsin-bearing post-Golgi membranes and causes cell death of transgenic Xenopus rods. Mol Biol Cell. 2001; 12:2341–2351. [PubMed: 11514620]

Nagy A, Rossant J, Nagy R, Abramow-Newerly W, Roder JC. Derivation of completely cell culture-derived mice from early-passage embryonic stem cells. Proc Natl Acad Sci USA. 1993; 90:8424–8428. [PubMed: 8378314]

Ocbina PJ, Anderson KV. Intraflagellar transport, cilia, and mammalian Hedgehog signaling: analysis in mouse embryonic fibroblasts. Dev Dyn. 2008; 237:2030–2038. [PubMed: 18488998]

Pan J, Snell WJ. Chlamydomonas shortens its flagella by activating axonemal disassembly, stimulating IFT particle trafficking, and blocking anterograde cargo loading. Dev Cell. 2005; 9:431–438. [PubMed: 16139231]

Pazour GJ, Bloodgood RA. Targeting proteins to the ciliary membrane. Curr Top Dev Biol. 2008; 85:115–149. [PubMed: 19147004]

Pedersen LB, Veland IR, Schroder JM, Christensen ST. Assembly of primary cilia. Dev Dyn. 2008; 237:1993–2006. [PubMed: 18393310]

Petersen C, Fuzesi L, Hoyer-Fender S. Outer dense fibre proteins from human sperm tail: molecular cloning and expression analyses of two cDNA transcripts encoding proteins of approximately 70 kDa. Mol Hum Reprod. 1999; 5:627–635. [PubMed: 10381817]

Pugacheva EN, Jablonski SA, Hartman TR, Henske EP, Golemis EA. HEF1-dependent Aurora A activation induces disassembly of the primary cilium. Cell. 2007; 129:1351–1363. [PubMed: 17604723]

Rieder CL, Jensen CG, Jensen LC. The resorption of primary cilia during mitosis in a vertebrate (PtK1) cell line. J Ultrastruct Res. 1979; 68:173–185. [PubMed: 480410]

Rohatgi R, Milenkovic L, Scott MP. Patched1 regulates hedgehog signaling at the primary cilium. Science. 2007; 317:372–376. [PubMed: 17641202]

Rosenbaum JL, Witman GB. Intraflagellar transport. Nat Rev Mol Cell Biol. 2002; 3:813–825. [PubMed: 12415299]

Santos N, Reiter JF. Building it up and taking it down: the regulation of vertebrate ciliogenesis. Dev Dyn. 2008; 237:1972–1981. [PubMed: 18435467]

Schneider L, Clement CA, Teilmann SC, Pazour GJ, Hoffmann EK, Satir P, Christensen ST. PDGFRalphaalpha signaling is regulated through the primary cilium in fibroblasts. Curr Biol. 2005; 15:1861–1866. [PubMed: 16243034]

Tammachote R, Hommerding CJ, Sinders RM, Miller CA, Czarnecki PG, Leightner AC, Salisbury JL, Ward CJ, Torres VE, Gattone VH II, et al. Ciliary and centrosomal defects associated with mutation and depletion of the Meckel syndrome genes MKS1 and MKS3. Hum Mol Genet. 2009; 18:3311–3323. [PubMed: 19515853]

Tamplin OJ, Kinzel D, Cox BJ, Bell CE, Rossant J, Lickert H. Microarray analysis of Foxa2 mutant mouse embryos reveals novel gene expression and inductive roles for the gastrula organizer and its derivatives. BMC Genomics. 2008; 9:511. [PubMed: 18973680]

Tucker RW, Pardee AB, Fujiwara K. Centriole ciliation is related to quiescence and DNA synthesis in 3T3 cells. Cell. 1979; 17:527–535. [PubMed: 476831]

Vintersten K, Monetti C, Gertsenstein M, Zhang P, Laszlo L, Biechele S, Nagy A. Mouse in red: red fluorescent protein expression in mouse ES cells, embryos, and adult animals. Genesis. 2004; 40:241–246. [PubMed: 15593332]

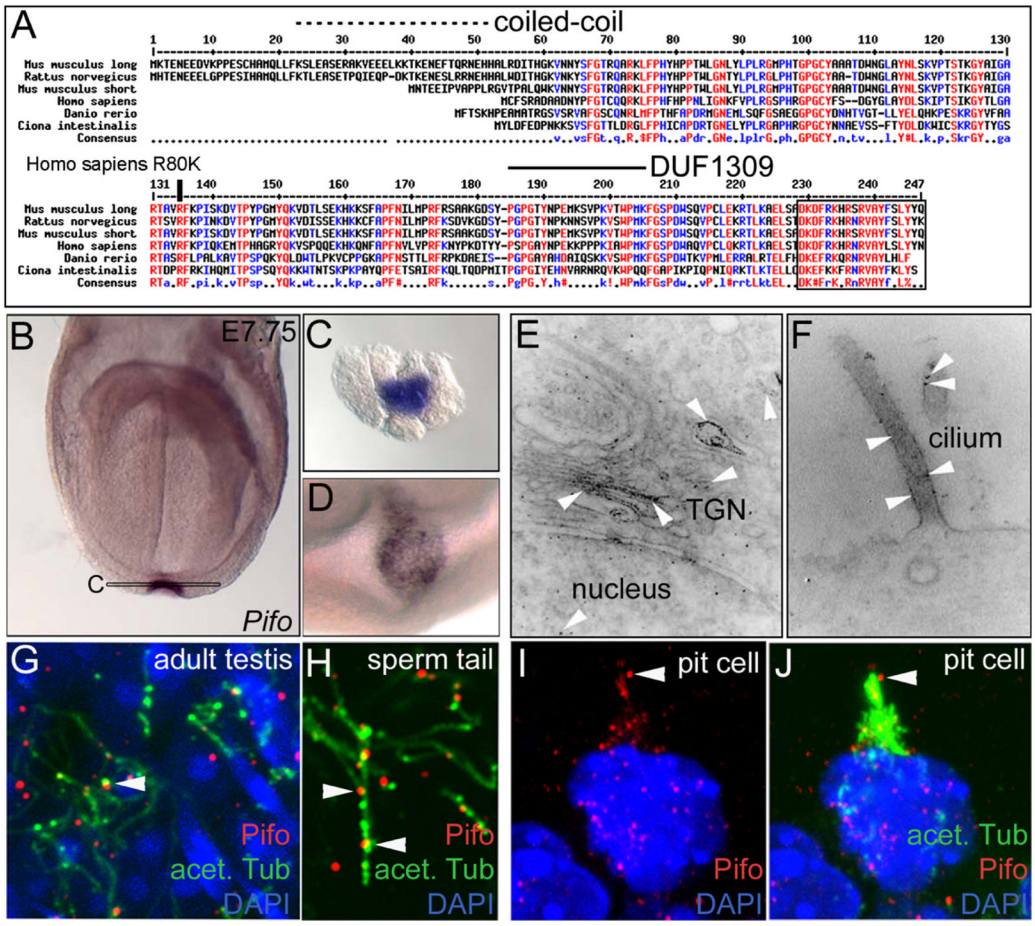


**Figure 1. Identification of Pifo as a Node and Ciliary Protein**

(A) Multiple species ClustalW protein alignment of Pifo reveals evolutionary conservation in chordates and conserved regions. N-terminal coiled-coil domain (dotted line) and the DUF1309 domain (solid line) are indicated. The boxed region shows the epitope for antibody production. The human R80K mutation is indicated. Whole-mount in situ hybridization shows expression of *Pifo* mRNA restricted to the ventral node pit cells at E7.75 in an anterior (B) and distal view (D). (C) Histological transverse section shows restricted expression of *Pifo* mRNA in node pit cells. Ultrastructural immuno-EM reveals localization of the Pifo protein to the nucleus and in vesicles of the TGN of node pit cells (E) and between the axonemal MTs and ciliary membrane of the cilium (F) at E7.75. Confocal coimmunolocalization reveals that Pifo is localized in parcels along the sperm tail (H) of adult mouse testis (G) and along the stabilized MTs of mouse node pit cells at E7.75 (I and J). Pifo in red, acetylated Tubulin (acet. Tub) in green, and DAPI in blue. See also Figures S1 and S2.

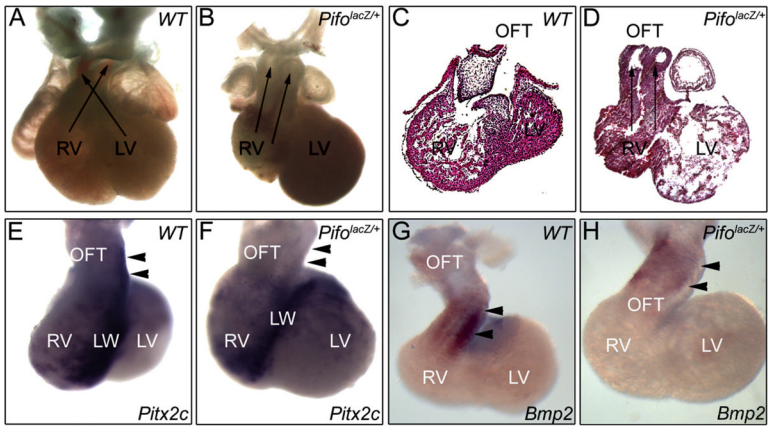


**Figure 2. Pifo Haploinsufficiency Causes Congenital Heart Disease in Mice**

(A) Frontal view of WT heart at E12.5. The right ventricle (RV) connects to the pulmonary artery, whereas the left ventricle (LV) connects to the dorsal aorta indicated by arrows. (B) *Pifo*$^{lacZ/+}$ hearts show DORV indicated by arrows and RV hypoplasia (compare ventricle size in [A] and [B]). Histological sections of *WT* (C) and *Pifo*$^{lacZ/+}$ hearts (D) confirm that both greater vessels of the OFT connect to the RV at E12.5. (E–H) Analysis of OFT marker genes by whole-mount in situ hybridization at E10.5. The left-sided expressed marker gene *Pitx2c* is expressed in the left OFT region and left lateral wall (LW) of the ventricle in *WT* embryos (E), but absent in the left OFT region in *Pifo*$^{lacZ/+}$ mutants (F). *Bmp2* is expressed throughout the OFT in *WT* embryos (G), but absent from the left OFT region in *Pifo*$^{lacZ/+}$ mutants (H).

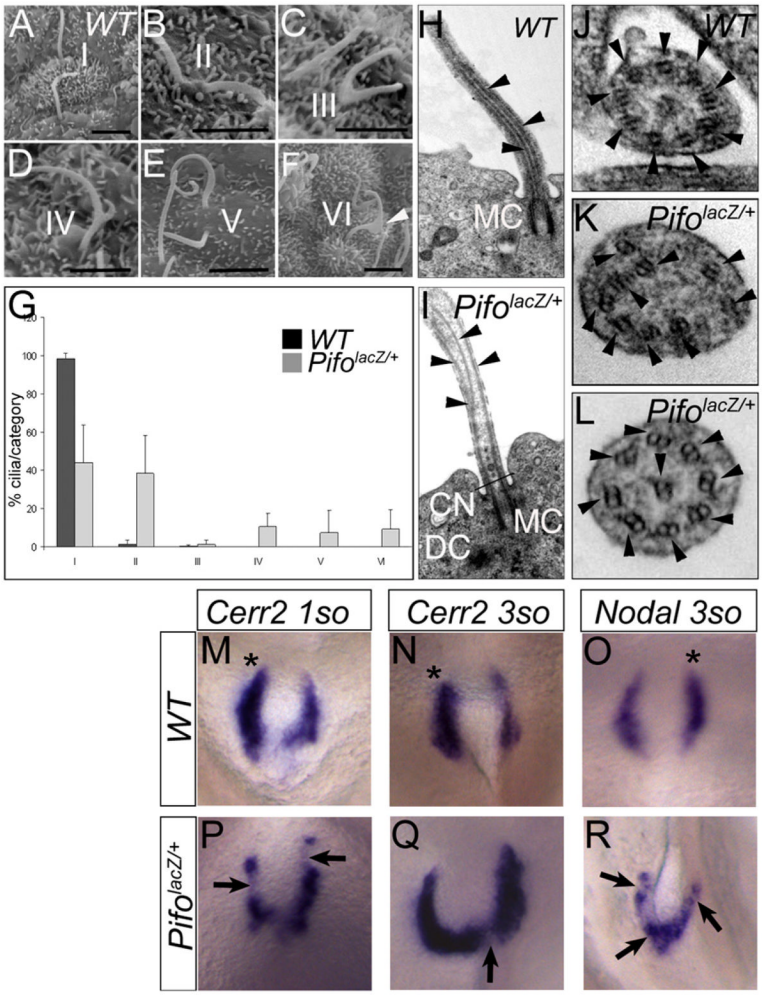


**Figure 3. Pifo Haploinsufficiency Causes a Unique Cilia Phenotype and Subtle LR Patterning Defects at the Node**

SEM reveals different categories of node cilia defects at the mouse node between E7.5 to 7.75. WT pit cells are monociliated (A, category I). In contrast, *Pifo* haploinsufficiency causes node cilia duplication (B, II), bifurcation (C, III), partial bifurcation (D, IV), duplication and malformation (E, V), and bulging (F, VI). (G) Summarized and quantified results of cilia phenotypes in three different WT (n = 270 cilia counted) and seven different $Pifo^{lacZ/+}$ embryos (n = 544 cilia counted), error bars show SD. TEM studies of *WT* (H and J) and $Pifo^{lacZ/+}$ mutant node cilia at E7.5 to E7.75 (I, K, and L). Node cilia show a 9 + 0 MT doublet arrangement indicated by arrowheads in a cross section through a *WT* cilium (J), but a disorganized MT architecture in $Pifo^{lacZ/+}$ cilia (K and L). Branching of MT doublet along the longitudinal axis is obvious in *WT* (H) and $Pifo^{lacZ/+}$ cilia (I) comparison. CN = ciliary necklace. (M–R) Whole-mount in situ hybridization analysis of the earliest LR asymmetry markers in the mouse at 1 to 3 somite (so) stage. (M–O) In *WT* embryos, *Cerr2* and *Nodal* mRNA expression shows a horseshoe-like expression pattern around the node with higher expression on one side (indicated by an asterisks). (P–R) In $Pifo^{lacZ/+}$ embryos horseshoe-like expression pattern is interrupted and ectopic posterior expression is seen. The pictures show a distal view on the mouse node, anterior is up and the left-right axis is a mirror image. See also Figure S3.

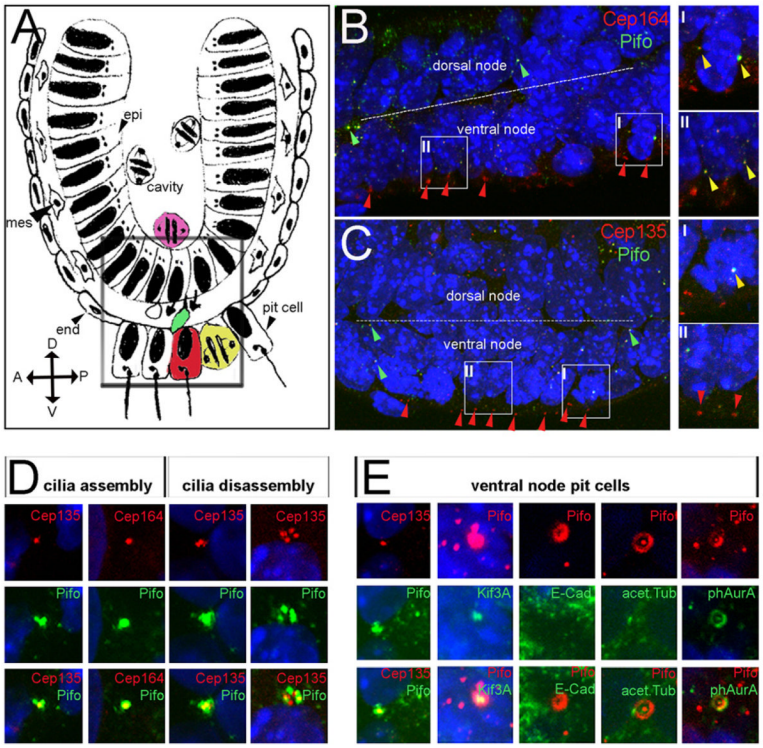


**Figure 4. Pifo Accumulates during Cilia Assembly and Disassembly at the Centrosome and Basal Body**

(A) Model of a gastrula-stage mouse embryo and ventral and dorsal node region (boxed area). Inner proliferating epiblast cells divide toward the amniotic cavity in the middle (purple cell). Cells that leave the epibast epithelium (green cell) exit the cell cycle and enter G0 to form primary ciliated node cells (red cells). Primary ciliated node cells divide in the ventral node epithelium (yellow cell). (B–E) Whole-mount colocalization studies of Pifo and centrosomal/basal body proteins in cilia-assembling and -disassembling node cells using confocal microscopy. (B) Pifo colocalizes with the appendage marker protein Cep164 in cilia-assembling (green arrowheads) and cilia-disassembling cells (yellow arrowhead in B, I), but not with primary ciliated node cells (red arrowheads in B and B, II). (C) Pifo colocalizes with the centriolar protein Cep135 in cilia-assembling intermediate cells (green arrowheads) and cilia-disassembling mitotic cells (yellow arrowheads in C, I and C, II), but is specifically excluded from the basal body of primary ciliated node cells (red arrowheads). (D) High-resolution colocalization study of Pifo with the centriolar marker protein Cep135 and the centriole appendage marker Cep164 in cilia-assembling and cilia-disassembling node cells. (E) High-resolution colocalization study of Pifo with centriolar protein Cep135, MT motor protein Kif3a, adherens junction protein E-Cadherin (E-Cad), activated AurA (phAurA), and the ciliary axoneme protein acetylated Tubulin (acet. Tub) in ventral node pit cells. Pifo is localized apical to the adherens junction at the base of the primary cilium in a ciliary necklace-like pattern and colocalizes with Kif3a, Cep135, and phAurA.

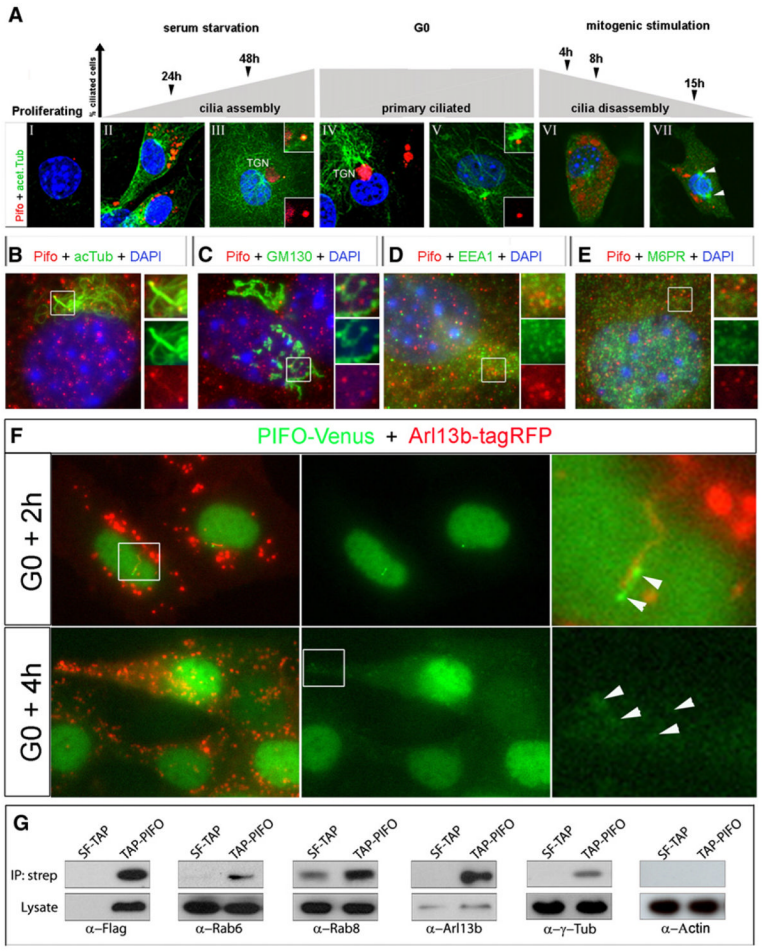


**Figure 5. Pifo Accumulates during Cilia Assembly and Disassembly and Associates with Ciliary Transport**

(A) Cell cycle-dependent Pifo accumulation was analyzed in PLC using immunocytochemistry. In proliferating culture, Pifo is hardly detectable (A, I). PLC cells were serum deprived for 24 to 48 hr to induce cilia assembly. During cilia assembly, Pifo vesicles strongly accumulate in the cytoplasm (A, II) and colocalize with the forming axoneme of the basal body (A, III). In primary ciliated cells Pifo either localizes to the TGN and overlaps with the basal body (A, IV) or is excluded from the mother centriole (A, V). After restimulation of PLC cells for 4 to 15 hr, Pifo accumulates in vesicles of the cytoplasm with levels peaking before mitosis (A, VI), which then decrease rapidly at the onset of mitosis (C, VII). (B–E) Colocalization study of Pifo with acetylated Tubulin (B), the *cis*-Golgi marker protein GM130 (C), the early endosome antigen1 EEA1 (D), and the endosome and TGN marker Mannose-6-phosphat receptor M6PR (E) in 4 hr cilia-disassembling PLC cells. (F) Live-cell imaging of PIFO-Venus and Arl13b-tagRFP in stably transfected IMCD3 cells reveals directed ciliary transport of PIFO-Venus along the cilium and in vesicles at 2 hr and 4 hr during cilia disassembly. Arrowheads indicate PIFO cargo and vesicles; boxed area is magnified. (G) Coimmunoprecipitation experiments in 4 hr cilia-disassembling HEK293T cells. The human SF-TAP-tagged PIFO was expressed in HEK293T cells and immunoprecipitated (IP) from lysates using Streptavidin (Strep)-affinity beads. Endogenous Rab6, Rab8, Arl13b, γ-Tubulin, and Actin were pulled down and detected after western blotting. Precipitation of bait protein was controlled by western

blotting using Flag antibodies. Five percent input is shown as loading and specificity control. See also Figures S4 and S5 and Movies S1 to S6.

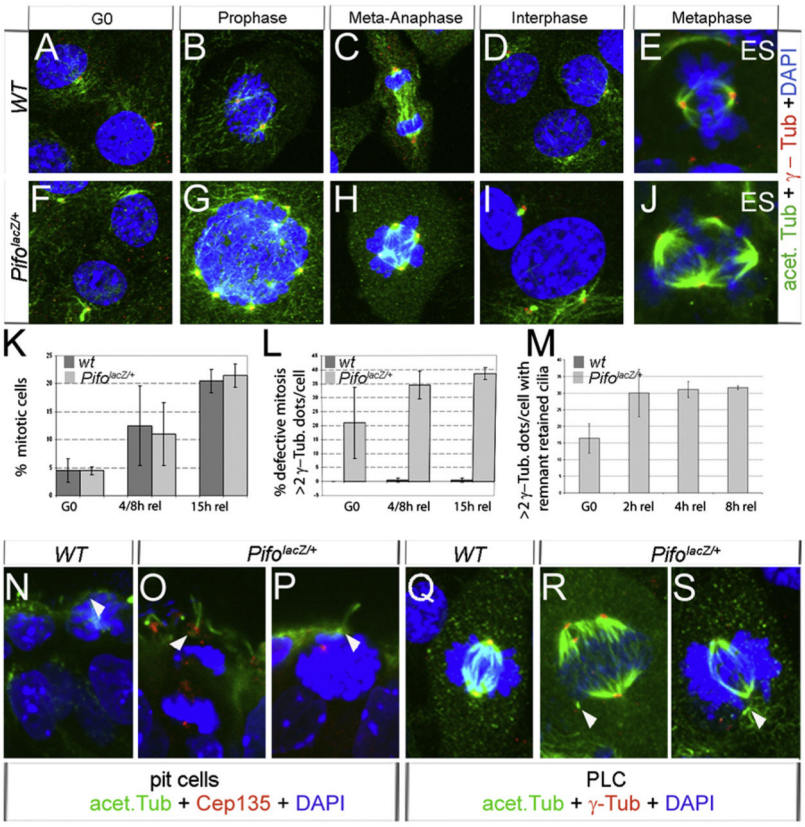


**Figure 6. Pifo Functions during Cilia Disassembly and Controls Basal Body Dislodging and Centriole Replication**

Analysis of Pifo function during cilia disassembly in WT (A–D) and *Pifo*$^{lacZ/+}$ (F–I) primary limb bud cultures. WT (A) and *Pifo*$^{lacZ/+}$ (F) primary fibroblast are 80% ciliated (K) and only 5% of cells divide (L) after 48 hr of serum starvation. After serum stimulation, WT and *Pifo*$^{lacZ/+}$ cells disassemble cilia (K) and reenter mitosis (L). In contrast to WT cells (B–D), *Pifo*$^{lacZ/+}$ cells show overreplication of centrosomes during S to prophase (G), multipolar spindles in metaphase (H), and cilia duplication after cytokinesis (I). Undifferentiated, proliferating ES cells contain around 10% to 15% ciliated cells and divide rapidly in culture (E). In *Pifo*$^{lacZ/+}$ ES cells, 2.5% dividing cells show multipolar spindles (J). (K), (L), and (M) represent the pooled data of three independent experiments in which 100 to 200 cells were counted, error bars show SD. Note that wt bars are not included in (M) as the value is zero. Ciliary disassembly studied in mitotic node cells (N–P) and PLC cells (Q–S) by immunolocalization studies. WT primary ciliated node cells (N) and PLC cells (Q) retract cilia and only possess two spindle poles, whereas *Pifo*$^{lacZ/+}$ node cells (O and P) and PLC cells (R and S) contain multiple spindle poles and fail to dislodge the cilium.

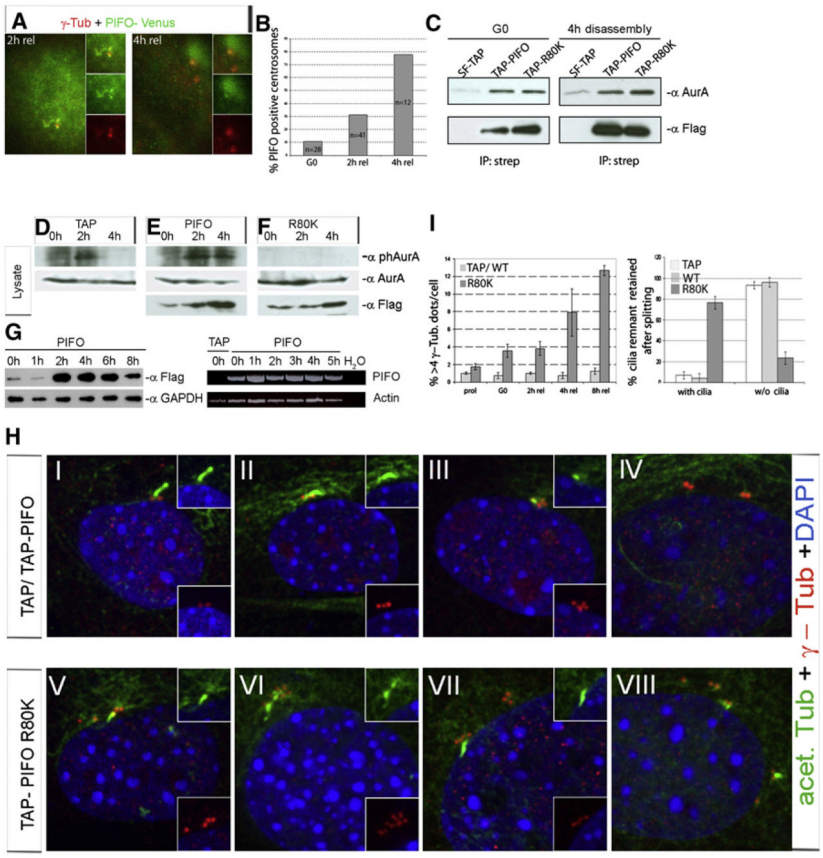


**Figure 7. PIFO-Mediated AurA Activation Is Necessary for Cilia Disassembly**

Translocation of PIFO-Venus to the γ-Tubulin-positive basal body/centrosome during cilia disassembly in stable transfected IMCD cells (A) and quantification (B). (C) Coimmunoprecipitation experiments in G0 and 4 hr cilia-disassembling HEK293T cells. The human SF-TAP-tagged PIFO and R80K PIFO were expressed in HEK293T cells and immunoprecipitated (IP) from lysates using Streptavidin (Strep)-affinity beads. Endogenous AurA was pulled down and detected after western blotting. Precipitation of bait protein was controlled by western blotting using Flag antibodies and the input levels of AurA are shown in (D–F) (G0 and 4 hr lane). (D–F) Overexpression of SF-TAP-tagged PIFO prolonged (E), whereas SF-TAP-tagged R80K PIFO (F) inhibited AurA phosphorylation as compared to SF-TAP control (D) in cilia-disassembling HEK293T cells. Expression of TAP-tagged constructs and overall AurA levels were controlled by western blotting using Flag and AurA antibodies, respectively. (G) Overexpressed SF-TAP-tagged PIFO in HEK293T cells is regulated on the posttranscriptional level as shown by PIFO RT-PCR analysis using Actin as a loading control (top panels) and western blotting using GAPDH as loading control (bottom panels). Note that no endogenous mRNA PIFO is expressed in mock-control transfected HEK293T cells (top panel, TAP). Cilia disassembly studied by immunolocalization studies in primary limb bud cultures overexpressing SF-TAP or SF-TAP-tagged WT (H, I–IV) and SF-TAP-tagged R80K PIFO (H, V–VIII). In contrast to WT PIFO overexpression, R80K PIFO causes centriole overreplication and failure to dislodge the basal body from the cilium. (I) represents the pooled data of three independent experiments in which 100 to 200 cells were counted, error bars show SD.